

Nonlinear theory of the Jeans instability in a cold nondissipative medium

A. V. Gurevich, K. P. Zybin, and Yu. V. Medvedev

P. N. Lebedev Physics Institute of the Russian Academy of Sciences, 117924 Moscow, Russia

(Submitted 13 April 1993)

Zh. Eksp. Teor. Fiz. **104**, 3369–3386 (October 1993)

The nonlinear dynamics of the Jeans instability in a cold nondissipative medium is studied analytically and numerically. It is found that as the system undergoes a transition to the equilibrium state an infinite number of caustics develop in it. It is shown that the equilibrium density distribution that arises has a singularity $\rho \propto x^{-4/7}$ at the center.

1. INTRODUCTION

As is well known, most of the mass in the universe resides in dark matter, which is shown convincingly by the rotational velocity profiles of galaxies, the motion of galaxies in clusters, etc.^{1,2} Unfortunately, we do not know what sort of particles make up this dark matter; we can assert with some confidence, however, that they are cold and interact very weakly with baryon material and each other. An important theoretical problem is therefore the study of the dynamics of such noninteracting and dissipationless material.

Previously we have studied the nonlinear dynamics of three-dimensional perturbations in nondissipative material in an expanding universe.^{3–5} There it was shown that for a broad class of initial perturbations (assuming only that the latter are not highly elongated along any single axis or two axes) a dissipationless gravitational singularity develops in the process of nonlinear compression and the subsequent kinetic mixing. This is a steady spherical structure of self-confined material, having a density singularity at the center. The density profile in a dissipationless gravitational singularity is accurately described by a power law:⁵

$$\rho \propto r^{-\alpha}, \quad \alpha \approx 1.7-1.8. \quad (1)$$

As can be seen from (1), the density singularity is integrable.

It is significant that the question of the nonlinear development of highly elongated or lenticular initial perturbations has not previously been studied. The main difference between the dynamics of these perturbations and that of the spheroidal perturbations discussed in Ref. 5 is that self-trapping of material near the dynamical singularity in the original compression of the latter does not take place. As a result material spreads out over a broad region and one may expect a very different, nonsingular steady structure to develop by the end of the kinetic mixing process.

The typical limiting case of this type of initial structure is one-dimensional. In these, self-trapping of matter naturally also does not occur near the $x=0$ singularity of the initial compression. Specifically, as shown in Ref. 3, near the singularity for $x \rightarrow 0$ the gravitational potential satisfies $\varphi \propto x^{4/3}$ and the flow velocity satisfies $V \propto x^{1/3}$. Consequently, the streaming kinetic energy $K \propto V^2 \propto x^{2/3}$ is much greater than the potential energy, so that no capture oc-

curs. It is the purpose of the present work to study the nonlinear dynamics of one-dimensional flows of self-gravitating cold dissipationless material.

Since there is no small parameter determining the rapid capture process near the singularity of the original compression, the analytical solution of the problem obtained in Refs. 4 and 5 is difficult. In the present work we therefore depend mainly on a numerical solution, supplemented by a detailed analytical critique. This enables us not only to study the steady state that develops as a result of kinetic mixing, but also to study the entire process of nondissipative nonlinear relaxation of the initial perturbation.

We can concisely summarize the main features of the process as follows. The nonlinear development of the Jeans instability results in a transition from the initial cold one-stream unstable hydrodynamic state of dissipationless gas to an equilibrium kinetic state trapped in the self-consistent gravitational field, with an infinite multiplicity of streams. The distribution function of the streams in the equilibrium state depends only on their energy. The streams proliferate because of successive tripling in the center of the cloud, which is accompanied by the generation of caustic waves expanding from the center. The flow therefore acquires a multicaustic nature. At each caustic located at a point $x_c(t)$, as is well known,⁶ the density of the material diverges $\rho \propto [x - x_c(t)]^{-1/2}$. Relaxation to the steady state results from the presence of an infinite number of caustics, which reduces the distance between them. Hence, despite the absence of material capture near the initial singularity, the steady distribution of material that develops in the center of the cloud is singular with a density

$$\rho \propto x^{-4/7}. \quad (2)$$

As in the three-dimensional case (1), the density singularity (2) is integrable. But the presence of an infinite number of caustics under nondissipative conditions implies the existence of infinite density fluctuations. Similar fluctuations occur, of course, in three-dimensional geometry.

Thus, in the completely nondissipative case, strictly speaking, no equilibrium state is reached. We see that a strong initial deviation from equilibrium does not disappear, but only breaks up into a multitude of small-scale fluctuations. However, the reduction in the scale of the perturbations, even though they are strong, enables us to distinguish an average equilibrium state because of their

integrability. If we analyze the concept of entropy, then it may turn out in our nondissipative mixing case that it is conserved, although in order to reach a genuine equilibrium state it should increase strongly. The excess entropy is contained in the nonequilibrium fluctuations.

2. INITIAL STAGE OF THE NONLINEAR DYNAMICS OF THE JEANS INSTABILITY

The initial process of the nonlinear dynamics of a cold nondissipative medium is described by the hydrodynamic equations:

$$\begin{aligned} \frac{\partial \rho}{\partial t} + \frac{\partial}{\partial x}(\rho V) &= 0, \\ \frac{\partial V}{\partial t} + V \frac{\partial V}{\partial x} + \frac{\partial \psi}{\partial x} &= 0, \\ \frac{\partial^2 \psi}{\partial x^2} &= \rho, \end{aligned} \quad (3)$$

where ρ is the density, V is the velocity, and ψ is the potential produced by the cold nondissipative material. In Eqs. (3) a system of units is used in which $4\pi\gamma=1$.

Equations (3) must be supplemented with initial conditions. As was shown in Ref. 4, without loss of generality they can be chosen in the form

$$\rho = \rho_0(x), \quad V = V_0(x) = 0. \quad (4)$$

Equations (3) can be integrated exactly. Specifically, substituting the third equation of the system (3) into the first and introducing the notation $y = \partial\psi/\partial x$ and using the mass conservation law we find

$$\begin{aligned} \frac{\partial V}{\partial t} + V \frac{\partial V}{\partial x} + y &= 0, \\ \frac{\partial y}{\partial t} + V \frac{\partial y}{\partial x} &= 0. \end{aligned} \quad (5)$$

Using the hodograph transformation we obtain an implicit solution of Eqs. (5):

$$\begin{aligned} t &= -V/y + M(y), \\ x &= -V^2/2y + H(y). \end{aligned} \quad (6)$$

The functions $M(y)$ and $H(y)$ are determined from the initial conditions (4). In our case we have

$$\begin{aligned} M(y) &= 0, \quad V = -ty, \\ x &= -(y/2)t^2 + H(y). \end{aligned} \quad (7)$$

Analysis of the solution (7) shows that the neighborhood of the density maximum plays the main role in the process of compressing the initial nonuniformity. It is clear that in the most general case the initial density can be represented near a maximum in the form

$$\rho_0 = \rho_{00}(1 - x^2/a^2).$$

Going over to new dimensionless variables

$$x \rightarrow (\sqrt{2}/\pi)(x/a), \quad \rho \rightarrow \rho/\rho_{00},$$

we can take $\rho_0(x)$ in the form

$$\rho_0 = \begin{cases} \cos(\pi x), & -1/2 \leq x \leq 1/2 \\ 0, & x < -1/2; x > 1/2. \end{cases} \quad (8)$$

The solution of (7), taking into account the initial condition (8), assumes the form

$$x = -(y/2)t^2 + \frac{1}{\pi} \arcsin(\pi y). \quad (9)$$

It is easy to show that the solutions (7) and (9) last only for a finite time. Specifically, at time $t = t_c = \sqrt{2}$ near the maximum density a singularity occurs.³

$$\begin{aligned} \rho &= \frac{1}{3} \left(\frac{6}{\pi^2} \right)^{1/3} x^{-2/3} = \rho_0 x^{-2/3}, \\ \psi &= \frac{3}{4} \left(\frac{6}{\pi^2} \right)^{1/3} x^{4/3} = \psi_0 x^{4/3}, \\ V &= -\sqrt{2} \left(\frac{6}{\pi^2} \right)^{1/3} x^{1/3} = -V_0 x^{1/3}. \end{aligned} \quad (10)$$

Numerical solution of the problem also yields a similar singularity. The solution is found by means of the particle-in-cell method. We analyze the dynamics of particles satisfying the kinetic equation

$$\begin{aligned} \frac{\partial f}{\partial t} + v \frac{\partial f}{\partial x} + \frac{\partial \psi}{\partial x} \frac{\partial f}{\partial v} &= 0, \\ \frac{\partial^2 \psi}{\partial x^2} &= \int_{-\infty}^{+\infty} f dv. \end{aligned} \quad (11)$$

It is easy to show by direct substitution that the kinetic equation (11) is equivalent to the hydrodynamic system (3) when the distribution function is given in the form

$$f = \rho(x,t) \delta[v - V(x,t)]. \quad (12)$$

The initial conditions for the distribution function $f(x,v,0)$ are chosen in accordance with (8) and (12) in the form

$$f(x,v,0) = \rho_0(x) \delta(v), \quad (13)$$

where $\rho_0(x)$ is given by Eq. (8).

In the numerical solution the length of the computational system $-1 \leq x_0 \leq 1$ is taken to be twice the size of the region occupied initially by the particles. The potential is assumed to be prescribed at the boundaries ($x = \pm 1$), so that by virtue of the symmetry of the problem we can assume $\psi(-1) = \psi(1) = 0$. The collection of particles was monitored, which revealed that not one particle left the region of the calculation over the whole time of the simulation. In the calculation we used 10^5 particles; the time step Δt was 0.004 and the mesh spacing was $\Delta x = 2/3840 \approx 5 \cdot 10^{-4}$. There were of order 50 particles per zone on the average, which amply ensured the required accuracy of the calculation.⁷

Since prior to the onset time $t_c = \sqrt{2}$ of the singularity we have the analytical solution (9), (10), by comparing the two we were able to check the accuracy of the numer-

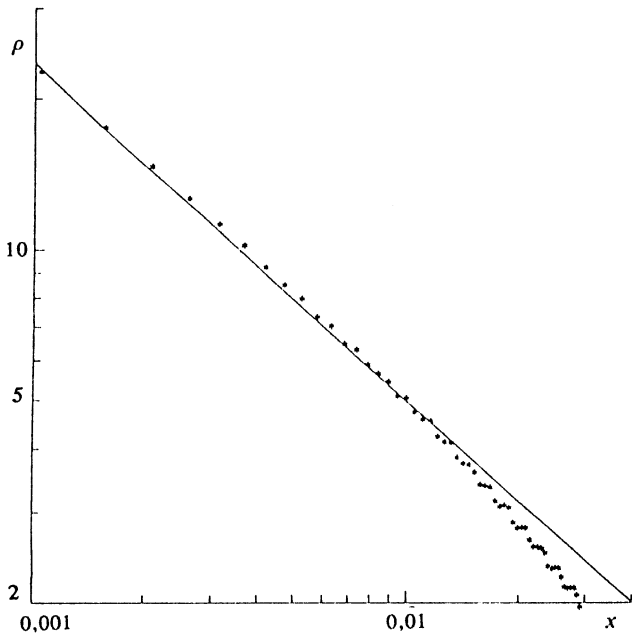


FIG. 1. Density and distribution at the time $t=\sqrt{2}$ when the singularity develops. The points represent the results of the numerical calculation and the straight line corresponds to the analytical dependence (10).

ical simulation, which was found to be quite good. In particular, as a result of the dynamical evolution of the initial distribution function (13) at time $t \approx 1.4142$ a very strong peak in the density develops at the center of the distribution. The corresponding dependence of $\log \rho$ on $\log x$ is shown in Fig. 1. The straight line corresponds to the analytical solution (10). It is evident that even in the immediate vicinity of the singularity the agreement between the numerical and analytical solutions is very good.

3. PROLIFERATION OF STREAMS

We proceed to study the behavior of the solution after the singularity $t > t_c$. For this purpose it is convenient to use in place of Eqs. (3) the equivalent equations (11) and (12). Now it is natural to regard the time $t=t_c$ at which the singularity occurs as the zero of time. Then the initial function $f(x, v, t_c)$ near the singularity $x=0$ is given by Eqs. (10), (12):

$$f(x, v, t) = \rho_0 x^{-2/3} \delta(v + V_0 x^{1/3}). \quad (14)$$

Now let us consider the behavior of the solution immediately following the singularity, i.e., for $\tau > 0$, where

$$\tau = t - t_c, \quad \tau > 0, \quad \tau \ll t_c.$$

We take into account the fact that in the region $x \ll 1$ of interest to us, it follows from Eq. (10) that the kinetic energy of the stream satisfies $V^2/2 \propto x^{2/3}$ and the potential energy satisfies $\psi \propto x^{4/3}$, i.e., the potential energy is substantially less than the kinetic. This means that the last term in Eq. (11) is unimportant, so that to lowest order we can disregard it. In this approximation the solution of Eq. (11) takes a simple form:

$$f(x, v, t) = f(x - v\tau, v, 0). \quad (15)$$

From (14) and (15) it then follows that

$$f(x, v, t) = \frac{1}{3} \left(\frac{6}{\pi^2} \right)^{1/3} (x - v\tau)^{-2/3} \times \delta \left(v + \sqrt{2} \left(\frac{6}{\pi^2} \right)^{1/3} (x - v\tau)^{1/3} \right). \quad (16)$$

It is significant that the argument of the δ function has three roots for $|x| < x_c = (2^{9/4}/3\pi)\tau^{3/2}$, $\tau > 0$. This means that in the neighborhood $\tau > 0$ of the singularity three streams develop in the flow. The distribution function (16) can therefore be rewritten in the form

$$f(x, v, t) = \sum_{i=1}^3 \rho_i(x, \tau) \delta[v + V_i(x, \tau)], \quad (17)$$

where the quantities

$$\rho_i = \frac{1}{3} \left(\frac{6}{\pi^2} \right)^{1/3} \frac{(x + V_i\tau)^{-2/3}}{|\xi'(V_i)|}$$

signify the density of the i th stream, and $V_i = V_i(x, \tau)$ are the roots of the equation

$$\xi(V_i) = V_i + \sqrt{2} \left(\frac{6}{\pi^2} \right)^{1/3} (x - V_i\tau)^{1/3} = 0.$$

Relation (17) is equivalent to the transition to multi-stream hydrodynamics. Specifically, using the representation of the distribution function in the form (17) we find from (11)

$$\frac{\partial \rho_i}{\partial t} + \frac{\partial}{\partial x} (\rho_i V_i) = 0,$$

$$\frac{\partial V_i}{\partial t} + V_i \frac{\partial V_i}{\partial x} + \frac{\partial \psi}{\partial x} = 0,$$

$$\frac{\partial^2 \psi}{\partial x^2} = \sum_i \rho_i. \quad (18)$$

In Eqs. (11) and (18) the caustics of the surface on which merging or splitting of the streams takes place play an important role. These are the points x_c . Specifically, as follows from (16) for $|x| < x_c$ there are three streams, while for $|x| > x_c$ there is one. At the points $x=x_c$ the derivatives of the merging velocity V_1 and V_2 have singularities

$$\left(\frac{\partial V_1}{\partial x} \right)_{x=x_c} \rightarrow +\infty, \quad \left(\frac{\partial V_2}{\partial x} \right)_{x=x_c} \rightarrow -\infty. \quad (19)$$

The densities ρ_1 and ρ_2 , along with the second derivative $\partial^2 \psi / \partial x^2$ of the field, vanish at the points x_c . However, the gravitational potential ψ and its first derivative remain continuous:

$$\begin{aligned} \rho_1|_{x \rightarrow x_c} &= \rho_2|_{x \rightarrow x_c} = \frac{1}{2} \left(\frac{\partial^2 \psi}{\partial x^2} \right)_{x \rightarrow x_c} \\ &= C(x_c, \tau) (x_c - x)^{-1/2}, \end{aligned}$$

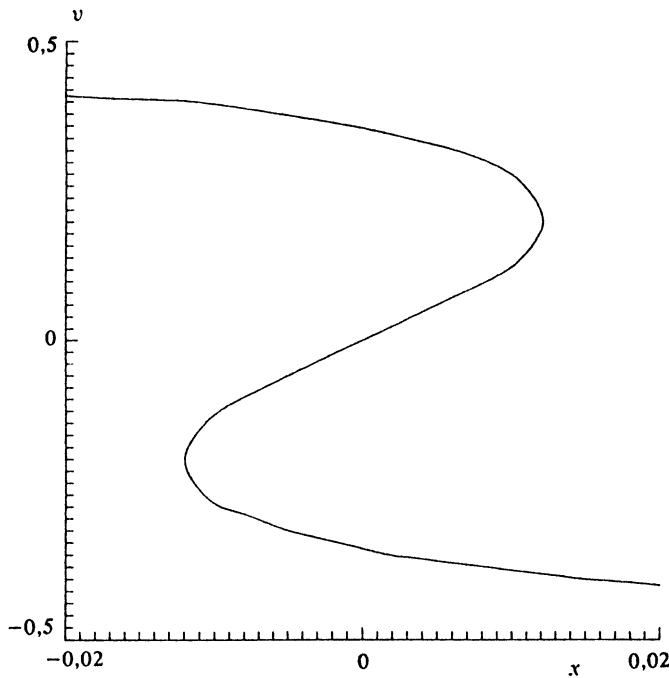


FIG. 2. The $v(x)$ phase plane at time $t=1.5$. The region in which the phase curve is three-valued corresponds to three-stream flow.

$$\left. \frac{\partial \psi}{\partial x} \right|_{x \rightarrow x_c + 0} = \left. \frac{\partial \psi}{\partial x} \right|_{x \rightarrow x_c - 0},$$

$$\psi(x_c + 0) = \psi(x_c - 0). \quad (20)$$

Conditions (19) and (20) can be written down at every point where the streams merge. They comprise a complete system of boundary conditions for Eqs. (18).

The results of the numerical solution, shown in Figs. 2 and 3, demonstrate the formation of a triple stream and the development of the density near caustics. As a result of the subsequent evolution the central stream gradually stops and begins to move in the opposite direction, and at some time it breaks, i.e., a singularity analogous to (10) develops all over again at the center of the distribution. After that a five-stream flow develops near the center, and caustics naturally arise which separate the five-stream and three-stream regions. In (x, v) space the flow acquires the form of a twisting spiral (Fig. 4). Subsequently the spiral twists still more and the number of streams near the center increases. Regions with different numbers of streams are separated by caustics. The density function is strongly indented, but the integrals of the density and the potential remain fairly smooth functions (20). This process is illustrated in Fig. 5.

4. THE STEADY STATE: ADIABATIC MODEL

Now we consider the state that develops in the process of prolonged mixing in the limit $t \rightarrow \infty$. As indicated above, in contrast to Ref. 5, in the present case the kinetic energy near the singularity is substantially greater than the potential energy at the time t_c of the initial singularity. Consequently there is no material trapped here, since immediately after the initial breaking the singularity disappears at the center, and the density distribution near the point $x=0$

becomes smooth (see Fig. 3). It is natural to expect that after prolonged mixing a similar smooth density distribution also arises, namely,

$$\rho = \rho_1 \left[1 - \left(\frac{x}{a_1} \right)^2 \right],$$

differing from the initial distribution (8) only by changes in the constants ρ_1 and a_1 .

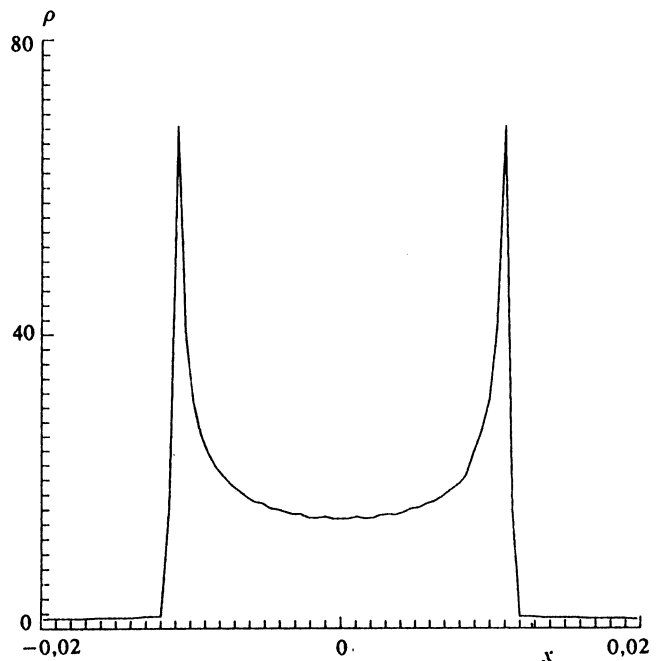


FIG. 3. The distribution of the density of the nondissipative material at time $t=1.5$. The density peaks near the caustics correspond to the distribution (20). The locations of the caustics correspond to the points at which the roots merge on the curve of Fig. 2.

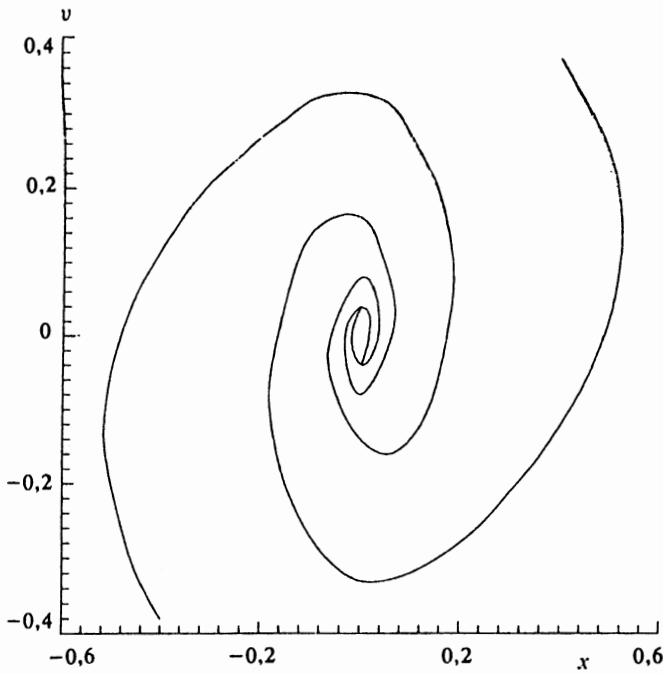


FIG. 4. The $v(x)$ phase curve corresponding to the region of five-current flow: $t=10.4$.

However, it does not work this way. The numerical calculation shows that with long calculation times material becomes concentrated near the center. The density $\rho(x)$ fluctuates strongly, so that this concentration is most clearly visible in a plot of the integrated density, i.e., the mass of material

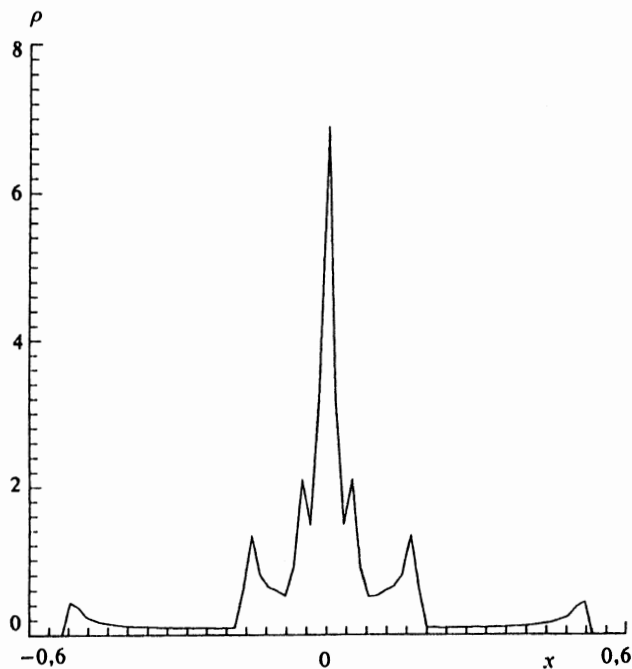


FIG. 5. Density distribution corresponding to the phase curve of Fig. 4. The plot clearly shows the central peak and the density peaks at the caustics.

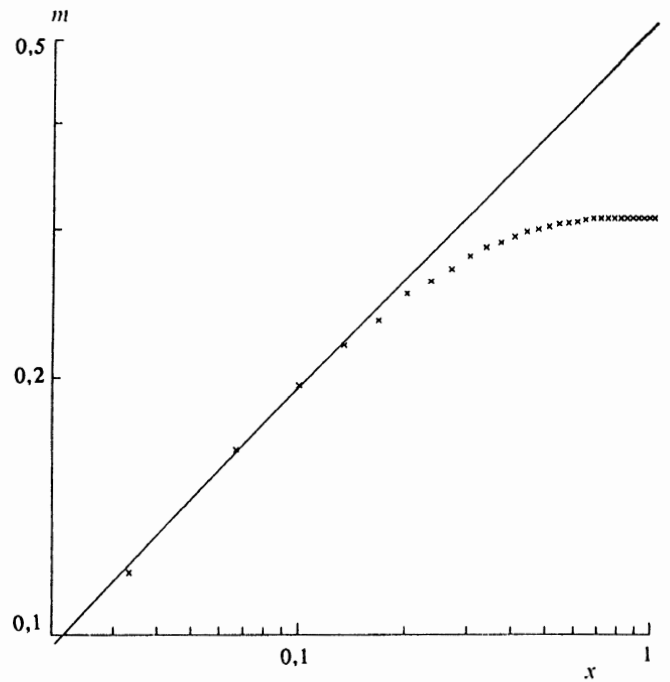


FIG. 6. The distribution of the integrated density (mass) of the material at time $t=23.6$. The straight line corresponds to the adiabatic model (32) and the x 's represent the result of the numerical simulation.

$$m(x) = \int_0^x \rho(x_1) dx_1; \quad (21)$$

see Fig. 6. For larger values $t > 10$ of the time the curve shown in this figure becomes essentially constant. Thus it shows a steady distribution of the integrated density. Evidently it differs considerably from the function $m(x) = \rho_1 x$ for $x \rightarrow 0$, which follows from (21). The figure also shows that in the steady state the average density $\bar{\rho}(x) = dm/dx$ grows rapidly as we approach the center $x=0$. Furthermore, in this region the fluctuations of $\rho(x)$ are enhanced, which says that the caustics of the singularities bunch up and implies that the potential of the average field differs considerably from $\psi - \psi_m \propto x^2$ in the limit $x \rightarrow 0$.

In order to explain the behavior of the singularities observed in the numerical experiment, it is necessary to perform some analysis of the process of multistream mixing at late times t . Here it is convenient to introduce instead of the variable v in Eq. (11) a new quantity, the adiabatic invariant I :

$$I = \int v dx = \int_{-x_m}^{x_m} \sqrt{2(\mathcal{E} - \psi)} dx. \quad (22)$$

Here \mathcal{E} is the energy $\mathcal{E} = v^2/2 + \psi$ of the stream; the reflection points $\pm x_m$ are determined by the condition $\mathcal{E} = \psi(x_m)$. For a given potential ψ expression (22) uniquely relates \mathcal{E} and the invariant I according to $\mathcal{E} = \mathcal{E}(I)$. In the new variables the system of equations (11) assumes the form

$$\frac{\partial f}{\partial t} \pm \sqrt{2(\mathcal{E} - \psi)} \frac{\partial f}{\partial x}$$

$$+\frac{\partial f}{\partial I} \int_{-x_m}^{x_m} \frac{\partial \psi(x,t)/\partial t - \partial \psi(x_1,t)/\partial t}{\sqrt{2(\mathcal{E} - \psi(x_1,t))}} dx_1 = 0,$$

$$\frac{\partial^2 \psi}{\partial x^2} = \int_{\psi}^{\mathcal{E}_m} \frac{f d\mathcal{E}}{\sqrt{2(\mathcal{E} - \psi)}}. \quad (23)$$

We also consider the approximation which we call the adiabatic model.¹⁾ This model is essentially the following. The mixing process consists of oscillations of the streams and the resultant appearance of multistream flows. In these oscillations the adiabatic invariant I is conserved if they are superimposed on a sufficiently slowly varying potential. The proliferation of the streams follows the initial singularity. The multistreaming region is bounded by the first caustic x_c : before it (for $|x| > x_c$) there is one stream, and after it (for $|x| < x_c$) there are three or more (Fig. 2). We assume that after the first caustic is passed mixing immediately occurs due to the rapid oscillations associated with the conservation of the adiabatic invariant. Then the form of the distribution function is determined from the conservation of the mass of material passing through the caustic:

$$\rho(x_c) \frac{dx_c}{dt} dt = f(I_c) \frac{dI_c}{dt} dt, \quad (24)$$

where x_c is the location of the caustic and I_c is the value of the adiabatic invariant on the caustic:

$$I_c = \int_0^{x_c} v dx = \frac{3}{4} V_0 x_c^{4/3} \quad (25)$$

From relations (22), (24), and (10) we find

$$f(I_c) = \left(\frac{3}{4}\right)^{3/4} \frac{\rho_0}{V_0} \left(\frac{I_c}{V_0}\right)^{-3/4}; \quad (26)$$

the constants ρ_0 and V_0 are defined in (10). Then by virtue of the adiabatic invariance for any value of I we have

$$f(I) = f(I_c) |_{I_c=I}. \quad (27)$$

The equation for the potential, taking into account (23) and (27), can be written in the form

$$\frac{\partial^2 \psi}{\partial x^2} = \int_{\psi}^{\mathcal{E}_c(t)} \frac{f(I) d\mathcal{E}}{\sqrt{2(\mathcal{E} - \psi)}}. \quad (28)$$

The system of equations consisting of (11) and (23) thus assumes the form (26), (27), and (28). Its solution in the limit $x \rightarrow 0$ is found in the form of a power law $\psi = \psi_1 x^\alpha$. Then according to (22), (26), and (27) we have

$$I = \frac{\mathcal{E}^{1/2+1/\alpha}}{\psi_1^{1/2}} C_0, \quad C_0 = \sqrt{2} \int_0^1 \sqrt{1-y^\alpha} dy,$$

$$f = \left(\frac{3}{4C_0}\right)^{3/4} \frac{\rho_0}{V_0} \left(\frac{\psi_1^{1/2}}{V_0}\right)^{-3/4} \left(\frac{\mathcal{E}}{\psi_1}\right)^{-3\alpha+6/8\alpha}. \quad (29)$$

Substituting (29) in (28) we finally find

$$\alpha = \frac{10}{I}, \quad \psi_1 = V_0^2 \left(\frac{49}{30} C_1 \left(\frac{3}{4C_0}\right)^{3/4} \frac{\rho_0}{V_0^2}\right)^{8/7};$$

$$C_0 = \sqrt{2} \int_0^1 \sqrt{1-y^{10/7}} dy = \frac{35\sqrt{\pi}}{12\sqrt{2}} \frac{\Gamma(7/10)}{\Gamma(1/5)} \approx 1.03;$$

$$C_1 = \frac{1}{\sqrt{2}} \int_1^\infty \frac{dy}{y^{9/10} \sqrt{y-1}} = \frac{\sqrt{\pi}}{2} \frac{\Gamma(2/5)}{\Gamma(9/10)} \approx 1.84.$$

Thus we see that the potential that develops as a result of multistream mixing,

$$\psi = \psi_1 x^{10/7}, \quad (30)$$

is a smooth function, which, however, differs considerably from x^2 in the limit $x \rightarrow 0$. The average density for $x \rightarrow 0$ has the singularity

$$\rho = \frac{39}{40} \psi_1 x^{-4/7}, \quad (31)$$

where the actual density in view of what was said above has strong fluctuations (sharp peaks) in the neighborhood of which Eq. (20) holds. But the integrated density, i.e., the mass calculated according to (31) and (21), by virtue of the integrability condition (20), is a smooth function

$$m(x) = (10/7) \psi_1 x^{3/7}. \quad (32)$$

In Fig. 6 the behavior of (32) is shown by a straight line. The agreement between the adiabatic model and the results of the numerical calculation is clearly evident.

The strong accumulation of particles toward the bottom of the potential well ($\mathcal{E} \rightarrow 0$) is also evident in the distribution function. According to (29) we have

$$f(\mathcal{E}) \propto \mathcal{E}^{-9/10}. \quad (33)$$

The distribution (33) also agrees with the results of the numerical calculation (see Fig. 7).

We see that the adiabatic model agrees well with the data from the numerical simulation. This agreement is probably a consequence of the relatively slow variation of the gravitational potential, whose fluctuations are small²⁾ (see Fig. 8). This gives rise to a numerical parameter which is responsible for the slow rate of change of the adiabatic invariant. Moreover, the oscillation period

$$T(\mathcal{E}) = \frac{dI}{d\mathcal{E}} = \frac{6}{5} \frac{C_0}{\psi_1^{7/10}} \mathcal{E}^{1/5} \quad (34)$$

vanishes for $\mathcal{E} \rightarrow 0$, which gives rise to rapid mixing of the streams in the vicinity of the bottom of the potential well.

5. BUNCHING OF CAUSTICS

In the steady state, as can be seen from (34), the oscillation period $T(\mathcal{E})$ near the bottom of the potential well ($\mathcal{E} \rightarrow 0$) approaches zero. This in turn implies that near the bottom caustics form at an increasingly rapid rate. This was shown above [see Eqs. (16), (17)]; the process by which caustics proliferate is the appearance in time of new zeros of the δ function. Hence the distribution function can always be expressed in the form

$$f(x, v, t) = \rho(x, t) \delta[v + V(x_0, v, t)]. \quad (35)$$

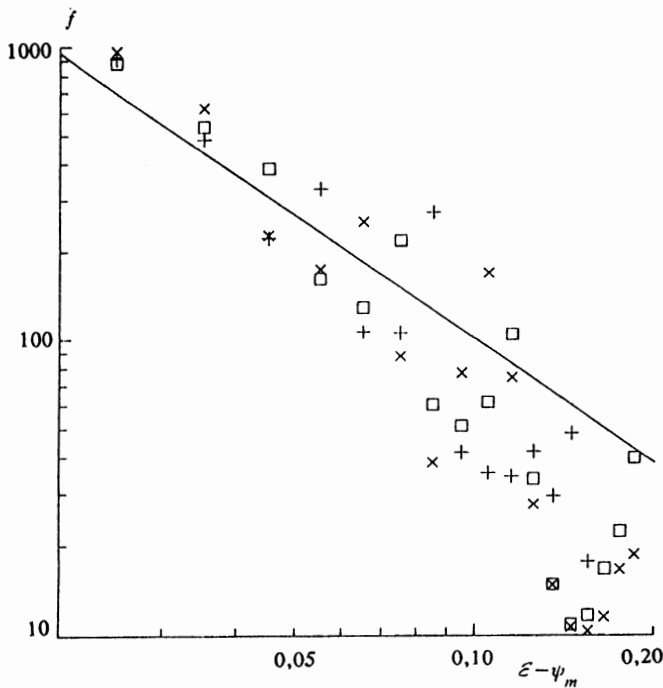


FIG. 7. The energy distribution function. The straight line corresponds to the adiabatic model of Eqs. (29) and (33), and the points correspond to the results of the numerical simulation at various times ($x-t=20$; $+ -t=21.6$; $\square -t=23.6$).

Here V is the initial velocity, expressed in terms of the initial position x_0 at the time t_c of breaking according to Eqs. (10):

$$V(x_0) = -V_0 x_0^{1/3},$$

where $x_0 = x_0(x, v, t)$ is the constant of motion defined by

$$\tau = t - t_c = \int_{x_0}^x \frac{dx_1}{(v^2 - 2\psi_1 x_1^{10/7})^{1/2}}. \quad (36)$$

It is assumed that asymptotically ($t \rightarrow \infty$) the motion takes place in the steady field (30).

Making a change of variables in (36), introducing in place of x_1 the quantity

$$\cos \theta = \sqrt{2\psi_1} x_0^{5/7} / v,$$

we find from (36)

$$v\tau = \frac{7}{5} \left(\frac{v^2}{2\psi_1} \right)^{7/10} \int_a^b \cos^{2/5} \theta d\theta, \quad (37)$$

where

$$a = \arccos(\sqrt{2\psi_1} x_0^{5/7} / v),$$

$$b = \arccos(\sqrt{2\psi_1} x_0^{5/7} / v).$$

At late times $\tau \gg t_c$, introducing the average value $\langle \cos^{2/5} \theta \rangle = q_0$, we find from (37)

$$v\tau = \frac{7}{5} \left(\frac{v^2}{2\psi_1} \right)^{7/10} (a-b) q_0. \quad (38)$$

The sequence of points at which caustics are located is determined by the conditions (19), which for large values of n are close to the points where the velocity vanishes (Fig. 4). However, in view of the symmetry of the picture under these conditions this sequence is similar to the sequence of points v_n on the $x=0$ axis. For this sequence we find from (38) using (10) the transcendental equation

$$v_n^{8/5} = V_0^3 (2\psi_1)^{-7/10} \sin^{7/5} \left[\frac{(2\psi_1)^{7/10} \tau}{q_0 v^{2/5}} \right]. \quad (39)$$

For $\tau \rightarrow \infty$ the solution of Eq. (39) agrees with the zeros of the sine function, so that

$$v_n \propto (\tau/n)^{5/2}, \quad n = 1, \dots, N. \quad (40)$$

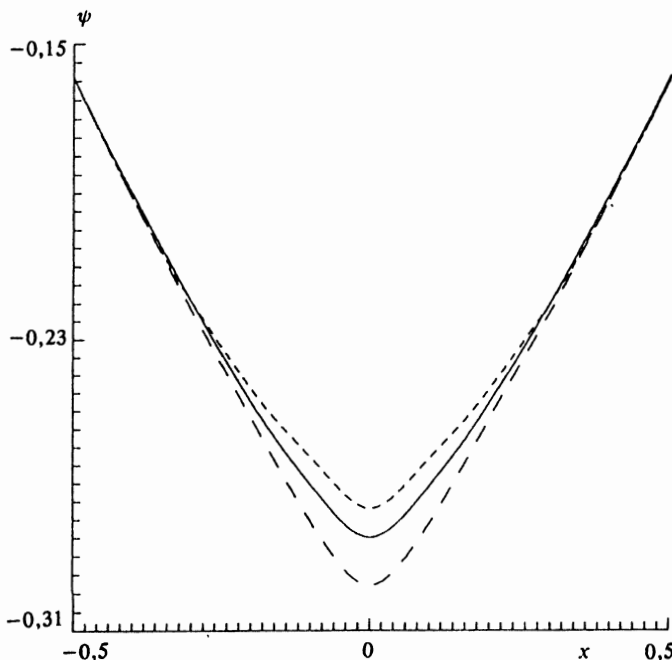


FIG. 8. Form of the potential at various times: $t=4.4$ (long dashes), $t=6$ (short dashes), and $t=24$ (solid trace).

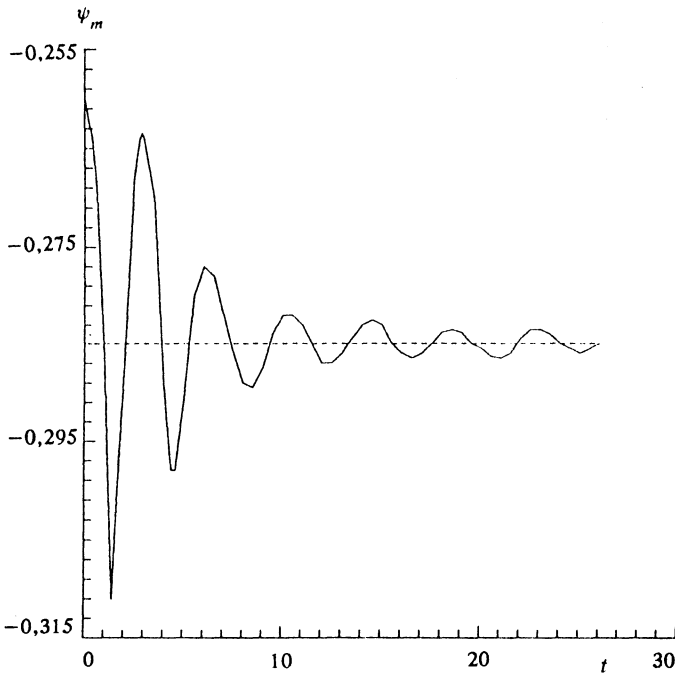


FIG. 9. Damping of the potential minimum versus time.

The total number N of caustics can be estimated from relation (39) if we use the fact that the sine cannot exceed unity:

$$N \approx V_0^{-3/4} (2\psi_1)^{7/10} \tau. \quad (41)$$

From this it is evident that the total number of caustics increases in proportion to the time τ . The relative distance between caustics, as follows from (40), is

$$\Delta v_n / v_n = (5/2)/n, \quad (42)$$

which decreases as a function of the number n . That is, caustics with large values of n bunch up near the center. Naturally, the same relations determine the positions x_n of the caustics. As the number of caustics increases the number of streams does also.

Thus, we see that the basis of the mixing process is the continual increase in the number of streams, as a result of which the system approaches the steady kinetic state. The significance of the increase in the number of caustics is that the spatial scale of the fluctuations is diminishing.

6. EIGENMODES

In the foregoing discussion we treated only small-scale caustic waves. In addition, the steady kinetic state (29) can be regarded as an equilibrium dynamical system. Deviations from the equilibrium position, including the initial state (8), must give rise to the excitation of eigenmodes of the system.

To describe the eigenmodes we write the distribution function f and the potential ψ in the form

$$f = f_0(\mathcal{E}) + f_1, \quad \psi = \psi_0(x) + \psi_1, \quad (43)$$

where f_0 and ψ_0 are the steady distribution function and potential. Substituting (43) in (11) we find

$$\frac{\partial f_1}{\partial t} + v \frac{\partial f_1}{\partial x} + \frac{\partial \psi_0}{\partial x} \frac{\partial f_1}{\partial v} + \frac{\partial \psi_1}{\partial x} \frac{\partial f_0}{\partial v} + \frac{\partial \psi_1}{\partial x} \frac{\partial f_1}{\partial v} = 0,$$

$$\frac{\partial^2 \psi_1}{\partial x^2} = \int_{-\infty}^{\infty} f_1 dv. \quad (44)$$

In the full equation (44) it is natural to distinguish the linear part

$$\frac{\partial f_1}{\partial t} + v \frac{\partial f_1}{\partial x} + \frac{\partial \psi_0}{\partial x} \frac{\partial f_1}{\partial v} + \frac{\partial \psi_1}{\partial x} \frac{\partial f_0}{\partial v} = 0,$$

$$\frac{\partial^2 \psi_1}{\partial x^2} = \int_{-\infty}^{\infty} f_1 dv. \quad (45)$$

This describes the characteristic modes of linear oscillation. The first mode is clearly evident in the oscillations of the potentials shown in Fig. 9. From the figure we see that the period T and accordingly the angular frequency ω of the first mode are equal to $T \approx 4.2$, $\omega \approx 1.50$. Here the time is expressed in units of the Jeans time t_c .

In view of the absence of dissipation in the system the linear oscillations must naturally be undamped, i.e., the eigenmodes λ_n of Eq. (45) must be purely imaginary. On the other hand, Fig. 9 clearly shows that the oscillation amplitude decreases. This is related to the fact that the amplitude of these potential oscillations is finite, and results from nonlinear mode interactions. To describe this process we expand the function f_1 in characteristic "ket" vectors $|g_n(x, v)\rangle$ of Eq. (45) and obtain

$$f_1 = \sum_n \exp(\lambda_n t) A_n(t) |g_n(x, v)\rangle, \quad (46)$$

where λ_n is the eigenvalue and $A_n(t)$ is the amplitude corresponding to the eigenmode $|g_n(x, v)\rangle$. Substituting ex-

pression (46) in (44) and multiplying Eq. (44) by the corresponding "bra" vector, we find an equation for the amplitude of the l -th mode

$$\frac{dA_l}{dt} = - \sum_{m,n} \exp[(\lambda_n + \lambda_m - \lambda_l)t] A_n A_m K_{l,m,n}, \quad (47)$$

where

$$K_{l,m,n} = \left\langle g_l \left| \int_0^x dx_1 \int_{-\infty}^{\infty} g_n(x,v) \frac{\partial}{\partial v} \right| g_m \right\rangle.$$

The equation for the amplitudes (47) permits us to find an asymptotic law for the damping of the amplitudes at late times t . Specifically, for $t \rightarrow \infty$ we have from (47)

$$\frac{dA_l}{dt} = - \sum_m A_{l-m} A_m K_{l,m,l-m}. \quad (48)$$

This type of equation for the mode amplitudes is a natural consequence of the quadratic behavior of the nonlinearity in Eqs. (44). Equation (48) has the obvious solution

$$A_l = C_l/t, \quad (49)$$

where the constants C_l satisfy the equation

$$\sum_m (C_{l-m} C_m K_{l,m,l-m} + \delta_{lm} C_m) = 0.$$

Thus we see that at late times the modes damp as $1/t$. This process is analogous to nonlinear Landau damping.⁸ The fundamental mode is most slowly damped; its dynamics can be estimated from the time dependence of the potential minimum. The process by which the potential damps is shown in Fig. 9. It agrees well with (49) and accordingly displays nonlinear behavior.

In conclusion we note that, since this system is conservative, both the damping of the modes and the decrease in scale of the caustics only mean that they are being pumped into smaller and smaller scales. In this sense it is useful to consider the total entropy of the system:

$$S = \int f \ln(e/f) dv dx. \quad (50)$$

In the initial state, as can easily be seen from (13), it is equal to $-\infty$. The dynamical process does not change the entropy. Consequently, the entropy must be equal to $-\infty$ at all times. This can easily be seen if we recall that the distribution function can be represented in the form (17).

In addition, if we consider the mixed kinetic state, then the entropy in it calculated using the steady distribution function (29) has the finite value

$$S_f = \frac{Q_0 \ln Q_0}{\beta+1} \psi_m^{\beta+1} + \frac{Q_0 \beta}{\beta+1} \psi_m^{\beta+1} \ln \psi_m - \frac{Q_0 \beta}{(\beta+1)^2} \psi_m^{\beta+1}.$$

In accordance with (29) we have $\beta=0.9$, ψ_m is the depth of the potential well, and

$$Q_0 = [3/(4C_0)]^{3/4} (\rho_0/V_0) (\psi_1^{1/2}/V_0) \psi_1^{0.9}.$$

Thus, we see that all the entropy in a mixed state is concentrated in giant small-scale fluctuations. In this sense we can speak of incomplete relaxation of the system to a mixed kinetic state due to the dynamical process considered here.

¹Unfortunately, there is no small parameter in this problem which would permit the theory of adiabatic trapping to be developed systematically. As we will see below, an adiabatic parameter develops only at late times [cf. Eq. (34)].

²As can be seen from the results of the numerical calculation, the greatest change in the potential occurs during the initial hydrodynamic compression. This is partly responsible for the choice of the matching condition (24) at the first caustic.

¹D. Burstein and V. S. Rubin, *Astrophys. J.* **297**, 423 (1985).

²E. J. Groth and P. J. E. Peebles, *Astrophys. J.* **270**, 20 (1983).

³A. V. Gurevich and K. P. Zybin, *Zh. Eksp. Teor. Fiz.* **94**, 3 (1988) [*Sov. Phys. JETP* **67**, 1 (1988)].

⁴A. V. Gurevich and K. P. Zybin, *Zh. Eksp. Teor. Fiz.* **94**, 5 (1988) [*Sov. Phys. JETP* **67**, 1957 (1988)].

⁵A. V. Gurevich and K. P. Zybin, *Zh. Eksp. Teor. Fiz.* **97**, No. 1, 20 (1990) [*Sov. Phys. JETP* **70**, 10 (1990)].

⁶Ya. B. Zel'dovich, *Astrophys. J.* **6**, 319 (1970).

⁷R. G. Hockney and J. W. Eastwood, *Computer Simulation Using Particles*, McGraw-Hill, New York (1981).

⁸E. M. Lifshitz and L. P. Pitaevskii, *Physical Kinetics*, Pergamon, Oxford (1981).

Translated by David L. Book